01 Jan 2014

High-Resolution Magnetic Susceptibility Measurements for Investigating Magnetic Mineral Formation during Microbial Mediated Iron Reduction

Estella A. Atekwana
Missouri University of Science and Technology, atekwana@mst.edu

Farag M. Mewafy

Gamal Z. Abdel Aal

D. Dale Werkema

et. al. For a complete list of authors, see https://scholarsmine.mst.edu/geosci_geo_peteng_facwork/1294

Recommended Citation

E. A. Atekwana et al., "High-Resolution Magnetic Susceptibility Measurements for Investigating Magnetic Mineral Formation during Microbial Mediated Iron Reduction," *Journal of Geophysical Research: Biogeosciences*, vol. 119, no. 1, pp. 80-94, American Geophysical Union (AGU), Jan 2014.
The definitive version is available at https://doi.org/10.1002/2013JG002414

AGU PUBLICATIONS

JGR

Journal of Geophysical Research: Biogeosciences

RESEARCH ARTICLE
10.1002/2013JG002414

Key Points:
- Microbial mediated iron-reduction can result in the precipitation of magnetite
- Higher magnetic susceptibility occurs within zones of iron-reduction
- Magnetic susceptibility is a viable tool in iron and carbon cycling studies

Correspondence to:
Estella A. Atekwana,
estella.atekwana@okstate.edu

Citation:
Atekwana, E. A., F. M. Mewafy, G. Abdel Aal, D. D. Werkema Jr., A. Revil, and L. D. Slater (2014), High-resolution magnetic susceptibility measurements for investigating magnetic mineral formation during microbial mediated iron reduction, *J. Geophys. Res. Biogeosci.*, *119*, 80–94, doi:10.1002/2013JG002414.

Received 8 JUN 2013
Accepted 17 DEC 2013
Accepted article online 19 DEC 2013
Published online 16 JAN 2014

High-resolution magnetic susceptibility measurements for investigating magnetic mineral formation during microbial mediated iron reduction

Estella A. Atekwana[1], Farag M. Mewafy[1,2], Gamal Abdel Aal[1,2], D. Dale Werkema Jr.[3], André Revil[4,5], and Lee D. Slater[6]

[1]Oklahoma State University, Stillwater, Oklahoma, USA, [2]Geology Department, Faculty of Science, Assuit University, Assiut, Egypt, [3]U.S. Environmental Protection Agency, Las Vegas, Nevada, USA, [4]Department of Geophysics, Colorado School of Mines, Golden, Colorado, USA, [5]ISTerre, CNRS, UMR CNRS 5275, Université de Savoie, Le Bourget du Lac, France, [6]Department of Earth and Environmental Sciences, Rutgers-Newark, Newark, New Jersey, USA

Abstract Disimilatory iron-reducing bacteria play an important role in the reduction of Fe(hydr)oxides and the production of secondary solid-iron mineral phases that can have magnetic properties. Magnetic susceptibility can therefore play an important role in identifying zones where microbial-mediated iron reduction is occurring. We investigated the magnetic susceptibility variations in a hydrocarbon-contaminated aquifer where methanogenesis and iron reduction are the main biogeochemical processes. Our objectives are to (1) determine the variability of magnetic susceptibility, (2) determine the hydrobiogeochemical controls on the magnetic susceptibility variability, and (3) evaluate the use of magnetic susceptibility as a viable technique for identifying zones where the coupling of iron and organic carbon cycling is occurring. Magnetic susceptibility data were acquired down 11 boreholes within contaminated and uncontaminated locations. We show that magnetic susceptibility values for boreholes within the free phase plume are higher than values for boreholes within the dissolved phase plume and background. Magnetic susceptibility values are highest within the zone of water table fluctuation with peaks predominantly occurring at the highest water table marks and are also coincident with high concentrations of dissolved Fe(II) and organic carbon content, suggesting that the zone of water table fluctuation is most biologically active. High magnetic susceptibility values within the vadose zone above the free phase plume are coincident with a zone of methane depletion suggesting aerobic or anaerobic oxidation of methane coupled to iron reduction. Our results suggest that magnetic susceptibility can be used as a viable tool in iron and carbon cycling studies.

1. Introduction

Iron is the fourth most abundant element on Earth and one of the most dominant redox active metals in the Earth's crust. Microorganisms reduce Fe(III) as ferrihydrite with either organic acids or H_2 as electron donor [*Lovley*, 1993; *Tuccillo et al.*, 1999]. Hydrocarbon-contaminated environments therefore provide excellent natural laboratories for investigating iron mineral biotransformations and the relationship between coupled carbon and iron biogeochemistry. Many studies have documented that iron-reducing bacteria can use hydrocarbon as a carbon source to reduce Fe(III) to Fe(II) [*Anderson and Lovley*, 2000; *Lovley et al.*, 1989] to form siderite [*Fredrickson et al.*, 1998; *Mortimer and Coleman*, 1997], magnetite [*Lovley*, 1990; *Lovley et al.*, 1987; *Mortimer and Coleman*, 1997; *Prommer et al.*, 1999; *Rijal et al.*, 2010], vivianite [*Fredrickson et al.*, 1998], ferroan calcite [*Baedecker et al.*, 1992], and green rust [*Fredrickson et al.*, 1998; *Parmar et al.*, 2001].

The bio-metallic minerals, in addition to other iron minerals, show a broad range of magnetic susceptibility (MS) responses between a highly positive response for ferrimagnetic minerals such as magnetite ($513–1116 \times 10^{-6}$ m^3 kg^{-1}), maghemite ($410–440 \times 10^{-6}$ m^3 kg^{-1}) [*Dunlop and Özdemir*, 2001], and greigite (320×10^{-6} m^3 kg^{-1}) to a low response for antiferromagnetic minerals such as hematite ($1.19–1.69 \times 10^{-6}$ m^3 kg^{-1}), goethite ($<1.26 \times 10^{-6}$ m^3 kg^{-1}), siderite (1.0×10^{-6} m^3 kg^{-1}), pyrite (0.3×10^{-6} m^3 kg^{-1}), and lepidocrocite ($0.5–0.75 \times 10^{-6}$ m^3 kg^{-1}) [*Dearing*, 1994]. Thus, magnetic susceptibility might be used as a tool to diagnose

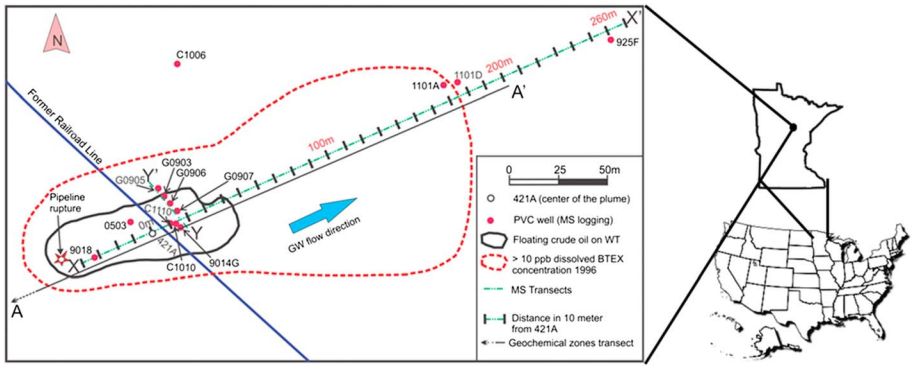

Figure 1. Study site showing location of boreholes and magnetic susceptibility transects X-X′ and Y-Y′ (shown on Figure 3). A-A′ shown on Figure 2.

biogeochemical zones where the coupling of carbon and iron cycling is occurring and provide a more holistic approach to subsurface investigation.

Magnetic susceptibility data from hydrocarbon-contaminated sites have documented zones of enhanced magnetic susceptibility within the smear zone (zone of water table fluctuation at hydrocarbon-contaminated location) coincident with the free phase (mobile or free liquids moving down through the unsaturated zone independent of the direction of flow of the groundwater or surface water) hydrocarbon plume [*Mewafy et al.*, 2011; *Rijal et al.*, 2010, 2012]. These studies suggest that magnetic susceptibility can be used as a tool to: (1) infer regions of hydrocarbon contamination, and (2) investigate intrinsic bioremediation by iron-reducing bacteria. A recent study by *Porsch et al.* [2010] suggests the utilization of MS to monitor the mineralogical transformations of magnetic iron minerals. The secondary mineralization pathways for the conversion of ferrihydrite to different iron mineral phases are controlled by the biogeochemical factors in the aquifer including Fe(II)/Fe(III) ratios, Eh, and pH [*Hansel et al.*, 2003, 2005; *Sumoondur et al.*, 2008]. Therefore, understanding the biogeochemical controls on the formation of magnetic minerals is critical for the development of magnetic susceptibility as a viable technique for the interrelationship between the geophysical response and biogeochemical settings.

In the present work, we extend the work of *Porsch et al.* [2010] and *Rijal et al.* [2010, 2012] by investigating the magnetic susceptibility variations at a hydrocarbon-contaminated aquifer near Bemidji, Minnesota, where methanogenesis and iron reduction are the main terminal electron acceptor processes [*Baedecker et al.*, 1993]. This site represents a natural laboratory available for investigating biophysicochemical processes associated with the intrinsic bioremediation of a crude oil spill. It is also characterized by an extensive geochemical and biological data base. Our objectives are to: (1) provide a detailed picture of the variability of MS at the field site, (2) determine what controls the variability of the MS, and (3) evaluate the use of MS as a viable technique for identifying zones of coupled iron and organic carbon biogeochemistry, using field based research.

2. Site History

The National Crude Oil Spill Fate and Natural Attenuation Research Site at Bemidji, MN (Figure 1), is a natural laboratory available for investigating biophysicochemical processes associated with the intrinsic bioremediation of a crude oil spill [*Cozzarelli et al.*, 2001; *Eganhouse et al.*, 1993]. The site geology consists of ~ 20 m thickness of moderately calcareous silty sand and outwash glacial deposits overlying clayey till of unknown thickness [*Bennett et al.*, 1993]. In August 1979, a high pressure crude oil pipeline ruptured, releasing 1,700,000 L of crude oil. Oil pooled in low-topographic areas (~2000 m^2) encompassing a total area of 6500 m^2 to the southwest of the pipeline and forming the north and south contaminated pools. In addition crude oil also sprayed to the southwest covering an approximately 7500 m^2 area of land (shown as spray zone on Figure 2). Our study is located on the north pool as it has been the focus of intensive geochemical [*Cozzarelli et al.*, 2010] and microbiological studies [*Bekins et al.*, 2001]. Seasonal water table fluctuation (~1 m annually) across the site enhances adsorption of free hydrocarbons (floating on the water table) onto the aquifer solids, resulting in a smear zone (dominated by free and residual hydrocarbon contamination) with variable thickness. According to *Essaid et al.* [2011], the north pool has a maximum oil saturation of 0.74 m in the down gradient part of the oil body with a smear zone of more than 2 m. The water table depth below ground

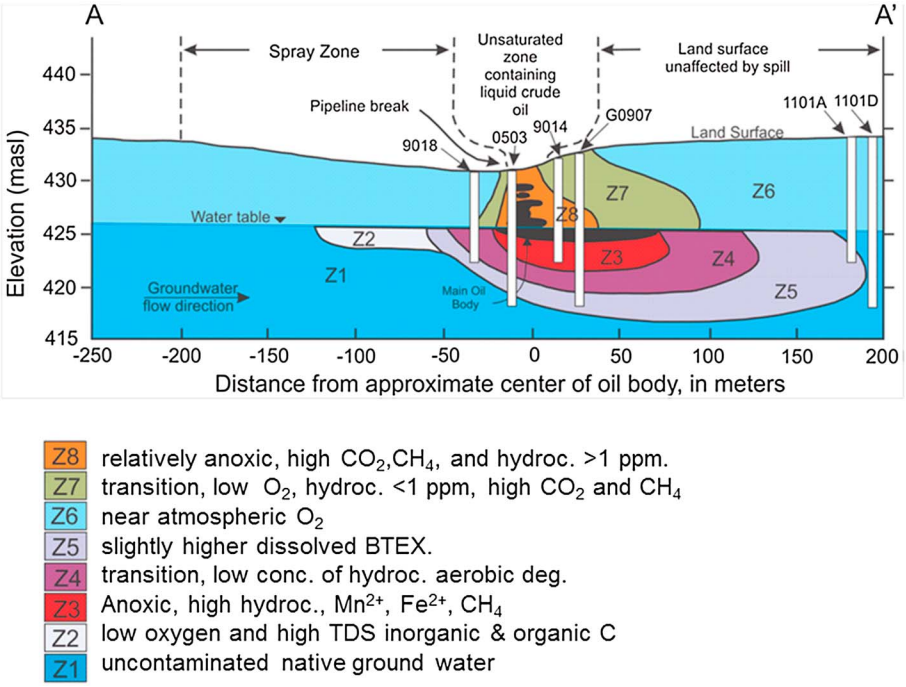

Figure 2. Characterized geochemical zones across the free phase plume and dissolved phase plume at the North oil pool of the study site in 1997 [modified from *Delin et al.*, 1998].

surface ranges from a minimum of 0 m (near an unnamed lake) to a maximum of 11 m with ~ 1 m seasonal fluctuation [*Delin et al.*, 1998].

The uncontaminated groundwater is aerobic with dissolved oxygen concentrations between 8 and 9 mg/L, dissolved organic carbon of 2.8 mg/L as C, and low levels of nitrate at 44.8 μg/L as N and sulfate at 2.9 mg/L [*Bennett et al.*, 1993]. Geochemical changes in the plume have been previously described by *Baedecker et al.* [1993] and *Cozzarelli et al.* [2010]. In the vicinity of the oil body, the aquifer is divided into anoxic, transition, and oxic (background) zones. Within the anoxic portion, hydrocarbons are predominantly oxidized by iron reduction [*Lovley et al.*, 1989] and methanogenesis [*Baedecker et al.*, 1993]. *Bekins et al.* [2001] identified two zones of methanogenic activity with CH_4 concentrations greater than 15 mg/L. The vadose zone vapor plume near the oil body has low O_2 (< 2%) and high CO_2 (>10%) and CH_4 (>15%) levels. Based on the estimation of the four physiologic microbial populations of aerobes, iron reducers, heterotrophic fermenters, and methanogens, *Bekins et al.* [2001] documented the progression from iron reduction to methanogenesis within the anaerobic portion of the contaminated aquifer.

Eight geochemical zones (Figure 2) have been identified at the North oil pool, five within the saturated zone (Zones 1–5), and three within the unsaturated zone (Zones 6–8) [*Baedecker et al.*, 1993; *Bennett et al.*, 1993; *Delin et al.*, 1998]. Zone 1 is characterized by the uncontaminated, oxygenated native groundwater. Zone 2 lies beneath the spray zone where the pipeline ruptured and is characterized by low oxygen concentrations and high concentrations of total dissolved inorganic and organic carbon. Zone 3 lies beneath the floating oil within the anoxic plume where the groundwater contains high concentrations of hydrocarbons, dissolved manganese (II), Fe (II), and methane. Zone 4 is a transition zone from anoxic to oxygenated conditions with low concentrations of hydrocarbons as a result of aerobic degradation processes. Zone 5 shows oxygenated water down gradient from the contamination plume that contains slightly higher concentrations of dissolved constituents, such as benzene, toluene, ethylbenzene, and xylene (BTEX). Zone 6 exhibits near atmospheric concentrations of O_2. Zone 7 denotes a transition zone with lower concentrations of O_2 (10–20%), hydrocarbon concentrations less than 1 part per million (ppm), and higher concentrations of CO_2 (0–10%) and CH_4 (0–10%). Finally, Zone 8 is relatively anoxic and contains maximum concentrations of CO_2 (>10%), CH_4 (>10%), and hydrocarbon (>1 ppm).

The geochemical and microbial studies suggest that iron reduction is an important terminal electron acceptor process occurring within the plume [e.g., *Baedecker et al.*, 1993]. In addition, dissimulatory

iron-reducing bacteria (DIRB) such as *Geobacter bemidjiensis sp*. and *Geobacter psychrophilus sp* occur in the contaminated aquifer [*Nevin et al*., 2005]. Several studies have investigated the mineralogy of the sediments within the site [*Baedecker et al*., 1992, 1993; *Tuccillo et al*., 1999; *Zachara et al*., 2004] and suggest that iron minerals in sediments include goethite, hematite, magnetite, ferrihydrite, and maghemite [*Bekins et al*., 2001].

3. Methodology

3.1. Magnetic Susceptibility Measurements

We conducted MS surveys along two, nearly perpendicular profiles: one in the direction of the groundwater flow (X-X′ from Figure 1) and the other nearly perpendicular to the groundwater flow direction (Y-Y′ from Figure 1). The field magnetic susceptibility data were acquired down 11 cased boreholes (shown as red dots in Figure 1) within locations of the free phase plume (9018, 0503, C1110, 9014G, G0907, G0906, and G0903), dissolved phase plume (1101A, 1101D, and G0905), and the uncontaminated location (925F) using a BSS-02B borehole magnetic susceptibility sonde (Bartington Instruments). All of the boreholes have polyvinylchloride (PVC) casings.

The BSS-02B is a borehole probe for measurement of magnetic susceptibility from 10^{-5} to 10^{-1} cgs and operates at 1.36 kHz. The magnetic susceptibility probe is characterized by high vertical and horizontal resolution up to 25 mm. The region of detection is situated 190 mm from the end. This probe can be operated in dry or water-filled boreholes. The sensitivity the magnetic susceptibility probe is 50 uT around the probe but decreases to 10 uT within 2 cm of the probe. The principle of operation of the probe (Operating manual, Bartington Instruments) is based on the magnetic state of a specimen, which is generally described by the following equation:

$$\mathbf{B} = \mu_o(\mathbf{H} + \mathbf{M}) \tag{1}$$

where:

B is the flux density of the specimen in Tesla.
μ_o is the permeability of free space. This is a constant ($4\pi \times 10^{-7}$).
H is the applied field strength in AT/m.
M is the magnetization of the specimen in Tesla.

Dividing through by **H**, we get:

$$\mu_r = \mu_o + \mu_o\kappa \tag{2}$$

where:

μ_r is the relative permeability of the specimen (dimensionless)
κ is the magnetic susceptibility of the specimen (dimensionless)

Rearranging, we get:

$$\mu_o\kappa = \mu_r - \mu_o \tag{3}$$

The sensor consists of a very high thermal stability oscillator for which a wound inductor is the principle frequency-determining component. When the inductor is surrounded only by air, the value of μ_o determines the frequency of oscillation. When the inductor is placed within the influence of the specimen to be measured, the value of μ_r determines the frequency of oscillation. Electronic circuitry digitizes the μ_o and μ_r-dependent frequency values with a resolution of better than one part in a million and computes the value of magnetic susceptibility.

In addition to the field measurements, a laboratory experiment was conducted to investigate the MS response of four common iron mineral phases (magnetite, hematite, siderite, and goethite) that possibly exist at the study site. The mineral specimens were obtained from the Geology Department at Oklahoma State University with purity up to 99%. The specimens were crushed into fine particles using a rock crusher and sieved to a size that passed through 0.15 mm sieve as this size represents the size range for magnetic minerals separated from the site. A portion of the sieved mineral specimen was mixed with fine sand 125–250 μm (0.1% dry weight or 0.23 $mg_{iron\ mineral}/g_{sand}$). The iron mineral-sand mixture was packed into a 10 cm^3 cup and volumetric MS measurements were obtained using a Bartington MS2 magnetic susceptibility meter and MS2B dual frequency sensor.

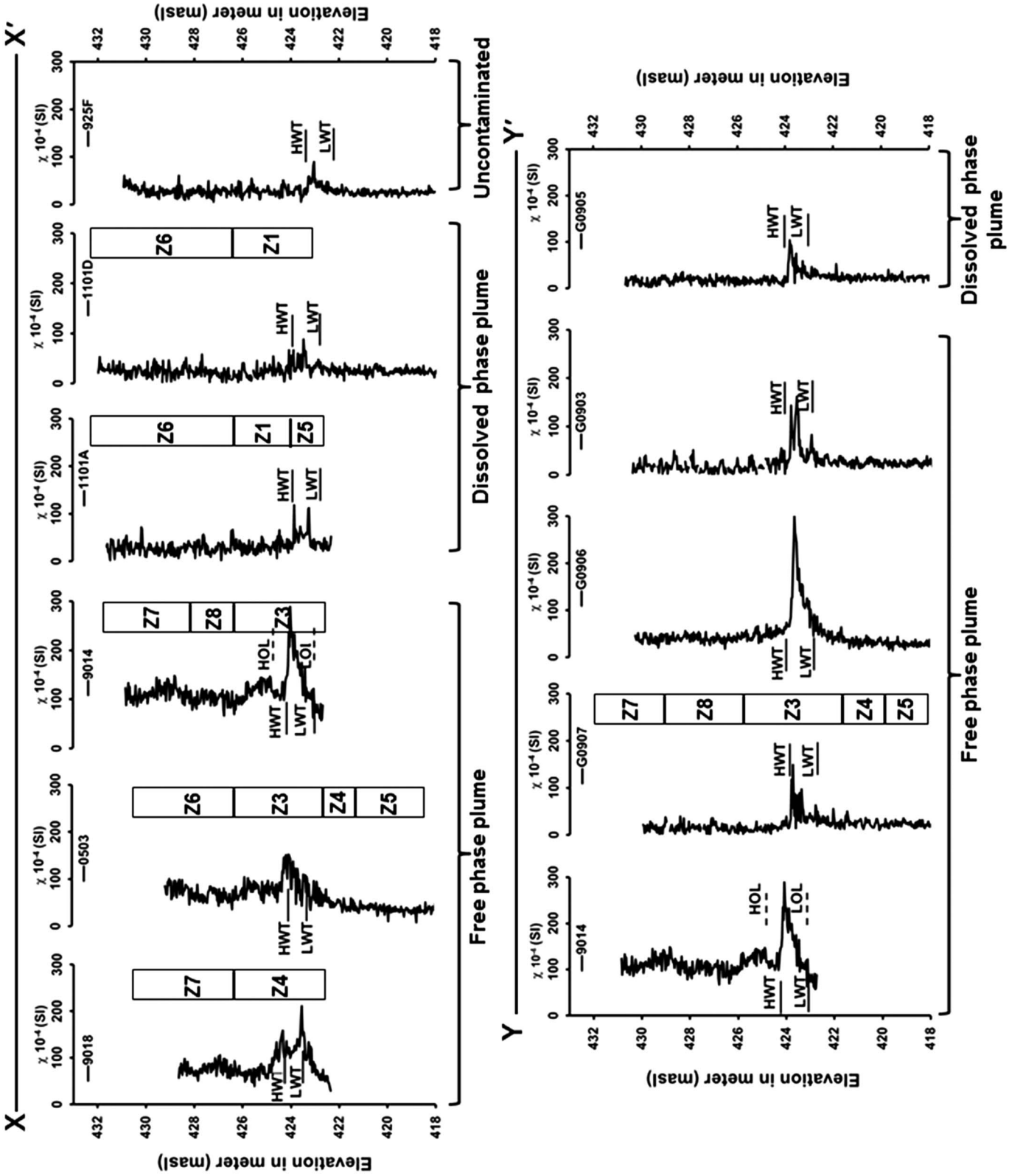

Figure 3. Magnetic susceptibility (values in SI) profile along transects X-X' and Y-Y' at the study site. Highest water table (HWT), lowest water table (LWT), highest oil level (HOL), and lowest oil level (LOL) between 2000 and 2009 are shown and the biogeochemical zones of Figure 2 are superimposed. Note the decrease in the amplitude and width of the anomaly from the fee phase oil plume to the dissolved phase oil plume and uncontaminated location.

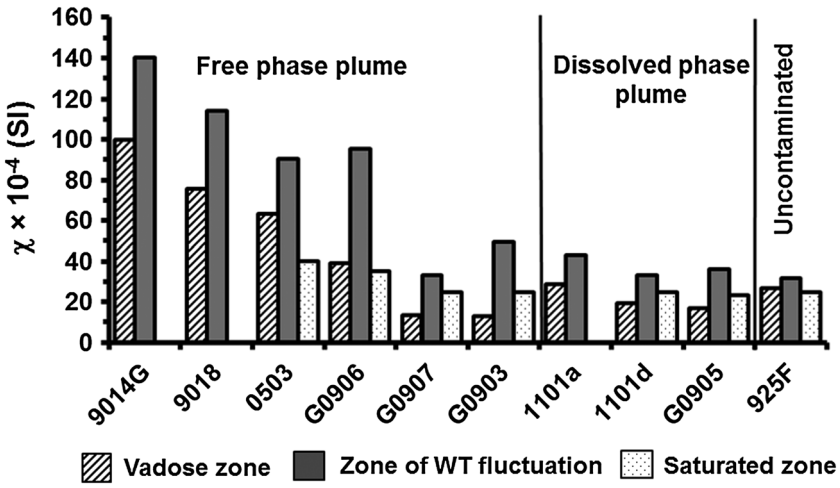

Figure 4. Histograms for the average magnetic susceptibility (values in SI) for the vadose zone, the zone of water table fluctuation, and the saturated zone along X-X′ and Y-Y′ transects. Notice the high MS magnitude for locations with free product compared to the dissolved product and uncontaminated location for both vadose zone and the zone of water table fluctuation. The label on the *x* axis represents the borehole numbers.

3.2. Characterization and Analysis of Sediments

3.2.1. Quantification of Magnetic Iron Minerals Content

Two cores (one from the contaminated and another from the uncontaminated location) retrieved from the field were sampled for isolation and characterization of the dominant magnetic iron mineral phases. Subsamples of sediments were taken at 5 to 15 cm intervals along the cores and air dried under vacuum at room temperature. The dried samples were used to quantify the magnetic iron mineral content using a bar magnet. The mass of magnetic iron minerals (particles) retained by the bar magnet was measured and the percentage of the magnetic-rich material per sample was determined. The magnetic susceptibility for the dried samples retrieved from the cores as well as the magnetic mineral content is presented in *Mewafy et al*. [2011]. In this study the magnetic susceptibility values ranged from 75 to 299×10^{-8} m^3kg^{-1} in the contaminated core to 40 to 145×10^{-8} m^3kg^{-1} for the uncontaminated core.

3.2.2. X-ray Diffraction (XRD) Analysis

X-ray powder diffraction (XRD) was performed on magnetic iron-rich samples isolated from contaminated core samples using a bar magnet in order to identify the magnetic iron mineral composition of the sediments. The phase and crystalline structure of the samples were confirmed by powder X-ray diffraction (XRD) using a Bruker D8 Advance diffractometer equipped with a LYNXEYE detector (D8-25 ADVANCE Bruker AXS GmbH). The diffractograms were obtained with CuKα radiation filtered by a 0.02 mm Ni foil to suppress the Kα lines, scanning in 2Θ with step size 0.02 degrees and 0.5 s per step. The operation voltage and current were 40 kV and 40 mA. The samples were placed in specimen holders for back-loading (sample reception 25 mm diameter by 0.6 mm depth). Phase identification was performed by matching the diffractograms with patterns from the International Centre for Diffraction Data (ICDD) PDF 2 Release 2011 Database version 2.1102.

3.2.3. Environmental Scanning Electron Microscope Imaging

Scanning electron microscope (SEM) imaging of the surface chemical composition and morphology of the bulk samples and magnetic fractions isolated from the contaminated core samples was carried out using an FEI Quanta 600 FEG integrated with electron backscattering diffraction (EBSD) system. The ESEM operating parameters varied depending on the surface characteristic being imaged and ranged from 2.5 to 8.0 kV, 5.9 to 11.1 mm, 700 to 3000×, for accelerating voltage, working distance, and magnification, respectively. Energy-dispersive X-ray spectroscopy (EDS) analyses were performed on the magnetic mineral particles to determine the mineral chemistry.

4. Results

4.1. Magnetic Susceptibility Measurements

Figure 3 shows the variability in magnetic susceptibility recorded in boreholes along the longitudinal (X-X′) and transverse profiles (Y-Y′) with superimposed geochemical zones (as shown in Figure 2). In general, we

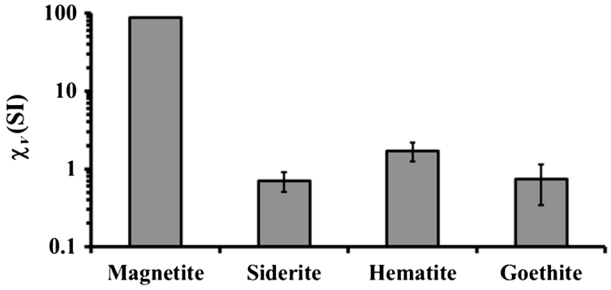

Figure 5. Magnetic susceptibility of different magnetic mineral phases from laboratory measurements. Magnetite dominates the magnetic susceptibility response.

observe a zone of higher (elevated) magnetic susceptibility ~1–1.5 m thick at the contaminated locations ~100–300 $\times 10^{-4}$ SI. This type of anomaly is not observed at the uncontaminated (background) location ~ 87.9 $\times 10^{-4}$ SI. Figure 3 shows that magnetic susceptibility values across the site show a marked increase within the zone of water table fluctuation with higher magnitude for the free phase plume compared to the dissolved phase plume as well as uncontaminated locations. This zone of enhanced magnetic susceptibility extends from the highest water mark to the lowest water mark and is coincident with geochemical zones 3 and 4 for the free phase plume and geochemical zones 1 and 5 for the dissolved phase plume. The magnetic susceptibility anomalies for most borehole locations show that the magnetic susceptibility values peak at the highest water mark, gradually decreasing toward the lowest water mark. In addition, some boreholes show a second peak at the lowest water mark (e.g., borehole 9018, 1101A, G0907, G0903). The magnetic susceptibility drops significantly within the saturated zone below the zone of WT fluctuation. For example, within borehole 0503 the magnetic susceptibility magnitude decreases from ~95 $\times 10^{-4}$ SI at 422.9 masl at the base of the water table fluctuation zone to ~46.5 $\times 10^{-4}$ SI at 420 masl within the saturated zone. The thickness of the zone of elevated magnetic susceptibility changes from ~1.7 m within the free phase plume (except for borehole G0907 in Y-Y′ profile) to ~0.6 m within the dissolved phase plume. We also observe a decrease in the magnitude of the magnetic susceptibility values down gradient from the free phase plume to the dissolved plume. For example, along profile X-X′, the magnetic susceptibility for borehole 9014, which is located about 15 m down gradient (i.e., within the free phase plume) from the center of the plume, has a magnitude peak of about 424 $\times 10^{-4}$ SI. In contrast, the maximum value recorded in well 1101D is 87.9 $\times 10^{-4}$ SI, which is located within the dissolved phase plume (~180 m from the core of the plume). At the background well 925F, which occurs further down gradient and is supposed to be outside the boundary of the dissolved phase plume, we still see a very small enhancement in magnetic susceptibility (89.58 $\times 10^{-4}$ SI) across the water table interface.

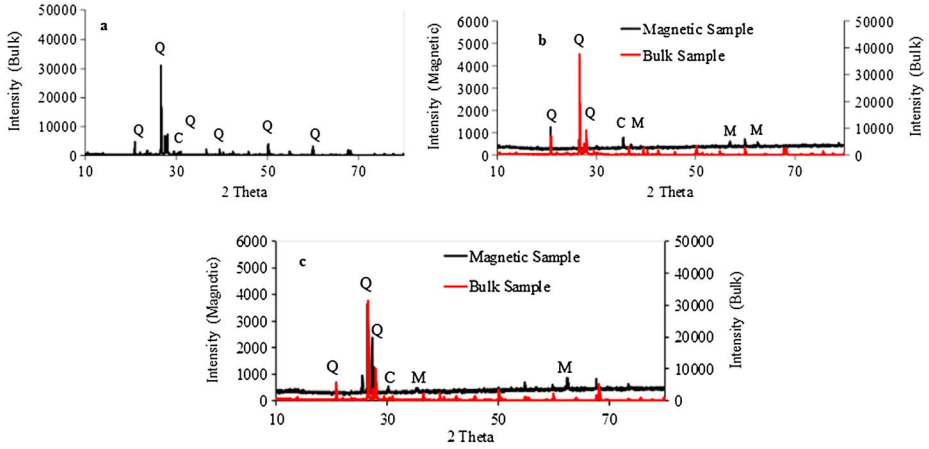

Figure 6. (a) XRD profiles of bulk mineral samples from the uncontaminated location and bulk and magnetic mineral samples isolated from the sediments using a magnet bar from a region of (b) high magnetic susceptibility and (c) low magnetic susceptibility. The results indicate that the magnetic minerals are mainly magnetite. Q — quartz, C — calcite, M — magnetite.

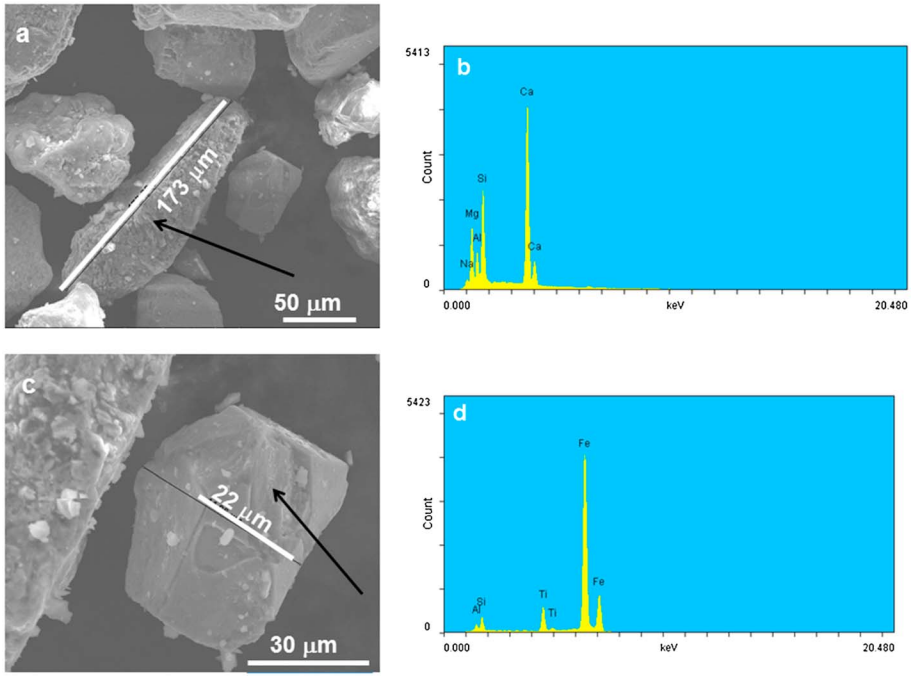

Figure 7. Scanning electron microscope (SEM) micrographs and energy-dispersive X-ray spectroscopy (EDS) analysis of magnetic-rich minerals separated from the sediments of contaminated core; (a and c) SEM micrographs from a region of low magnetic susceptibility and (b and d) EDS analysis of the surface layer.

Figure 3 reveals a higher magnetic susceptibility magnitude in the vadose zone above the free phase plume ~100×10^{-4} SI (9018, 0503, and 9014) and corresponding to geochemical zones 8 and 7, as compared to the vadose zone above the dissolved phase plume ~40×10^{-4} SI, which corresponds to geochemical zones 1 and 6. The only boreholes that deviate from this pattern are G0907 and G0903, which are within the free phase

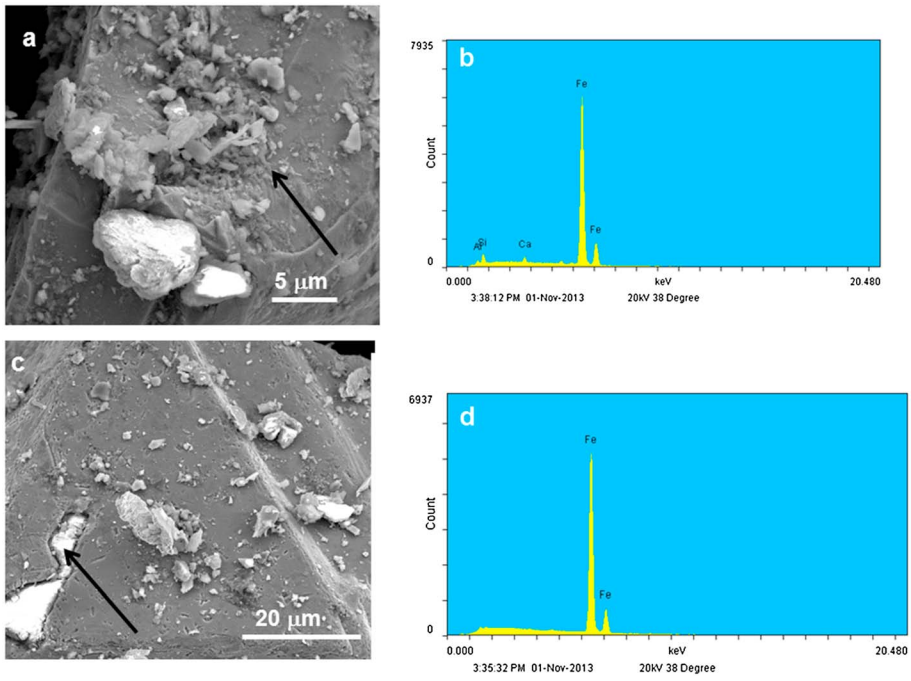

Figure 8. Scanning electron microscope (SEM) micrographs and energy-dispersive X-ray spectroscopy (EDS) analysis of magnetic-rich minerals separated from the sediments of contaminated core using a bar magnet; (a and c) SEM micrographs from a region of high magnetic susceptibility and (b and d) EDS analysis of the surface layer.

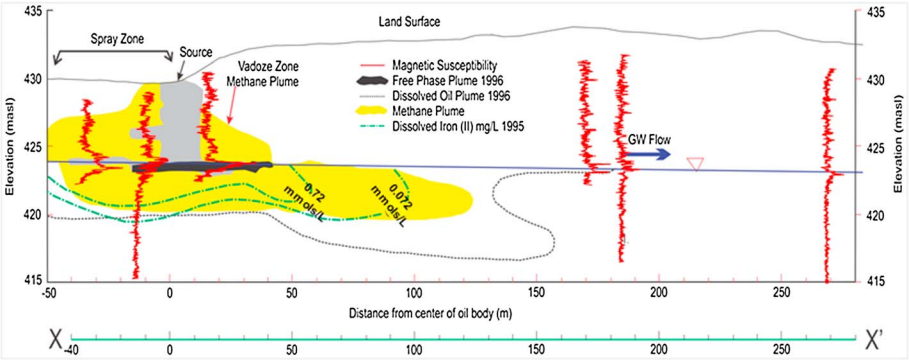

Figure 9. Magnetic susceptibility profiles superimposed on the free phase, methane and dissolved phase plumes and dissolved Fe (II) along transect X-X' [modified from *Cozzarelli et al.*, 2001].

plume. The magnetic susceptibility drops significantly within the saturated zone below the WT fluctuation zone ~31×10^{-4} SI and corresponding to geochemical zones 4 and 5 for the free phase plume locations.

Figure 4 shows the average magnetic susceptibility values of the vadose zone (2 m interval above the WT fluctuating zone), the zone of WT fluctuation, and below this zone (2 m interval). This figure clearly demonstrates, except for boreholes G0907 and G0903, that magnetic susceptibility measurements from within the free phase plume location display higher magnitude compared to magnetic susceptibility measurements from within the dissolved phase plume and uncontaminated locations. Also, the average values from within the zone of WT fluctuation suggest that this zone of magnetic susceptibility is about 4 times higher (90 to 140×10^{-4} SI) for most of the free phase plume locations (9018, 503, 9014, and G0906) compared to 31–43×10^{-4} SI at the dissolved plume locations (1101A, 1101D, and G0905). Additionally, the magnetic susceptibility magnitudes are higher at locations below the free phase plume (~46.5×10^{-4} SI at 420 masl for boreholes 0503 and G0906) compared to the dissolved phase plume (~26×10^{-4} SI at 420 masl for boreholes 1101D and G0905).

Figure 5 shows the laboratory magnetic susceptibility results of the 0.1% magnetic mineral-sand mixtures. The magnetic susceptibility (87.9 SI) response of magnetite dominates the magnetic susceptibility response of all the other minerals (0.75 SI for siderite; 1.7 SI for hematite; and 0.74 SI for goethite).

4.2. Characterization and Analysis of Sediments

The isolated magnetic iron-rich mineral grains range in size from 15 μm to 500 μm. The percentage of the magnetic iron-rich minerals (by dry weight) in the uncontaminated core varies from 0.07% to 0.22% with an average value of 0.14%. In contrast, the contaminated core showed relatively high percentages of magnetic-rich minerals ranging from 0.19% to 0.44%, reaching a maximum within the zone of water table fluctuation and coincident with higher magnetic susceptibility [*Mewafy et al.*, 2011]. According to the $^{o}2\theta$ and intensity values, the XRD patterns of samples from the uncontaminated core (Figure 6a) are dominated by quartz (Q) and some calcite (C). XRD patterns from the contaminated sediments from a region of high magnetic susceptibility (Figure 6b) and lower magnetic susceptibility (Figure 6c) suggest the presence of quartz and calcite as the nonmagnetic fractions with magnetite (M) as the dominant solid magnetic iron mineral phase. Figures 7 and 8 show SEM micrographs of the magnetic iron minerals from the contaminated location within a region of low magnetic susceptibility (Figure 7) and from the zone of peak magnetic susceptibility (Figure 8). The SEM micrographs of the mineral grain surfaces varied according to location. In the zone of high magnetic susceptibility, mineral surfaces were covered with precipitates (Figures 8 a and 8c). EDS analyses of the coating layer suggested Fe-containing phase (Figures 8b and 8c). In zones of low magnetic susceptibility, SEM also showed precipitation (Figures 7a and 7c) and EDS analyses suggest Si, Al, Ca, Mg, Al, Na (Figure 7b), and Fe (Figure 7d).

5. Discussion

5.1. Magnetic Mineral Phases

The variability in magnetic susceptibility values both vertically and laterally appears to be related to the presence of hydrocarbon contamination (Figure 9) as well as the geochemical zones shown in Figure 2. For

microbes to aerobically or anaerobically degrade oil, the reduction of an electron acceptor is required [*Schink*, 2005]. Ferrihydrite can be reduced to Fe (II) when aromatic hydrocarbon oxidation is coupled to iron reduction [*Anderson and Lovley*, 2000; *Lovley et al*., 1989]. This process can lead to the precipitation of a variety of ferrous minerals. X-ray diffraction (XRD) analyses of the separated magnetic iron mineral grains suggested that magnetite was the dominant solid mineral phase within the zone of peak magnetic susceptibility (Figure 6b). Previous studies at the site have documented the depletion of ferrihydrite toward the center of the plume with the enrichment of siderite, magnetite, and ferroan calcite [*Baedecker et al*., 1993; *Tuccillo et al*., 1999; *Zachara et al*., 2004]. Although siderite and ferroan calcite could have constituted part of the iron mineral phases isolated from the aquifer, further analysis suggests that small amounts of magnetite in sediments dominate the magnetic susceptibility response relative to the combined effect of all other iron mineral phases (Figure 5). This is not surprising as magnetite is ferrimagnetic, with very high magnetic susceptibility 10,000 – $57{,}000 \times 10^{-4}$ SI [*Dearing*, 1994]. In contrast, iron carbonates such as siderite are less magnetic (13–110×10^{-4} SI) [*Dearing*, 1994; *Jacobs*, 1963].

The SEM imaging of the magnetic minerals within the contaminated zone revealed variability in the character of the mineral surfaces within the presence of the hydrocarbon-contaminated zone (Figure 8). Within zones of high magnetic susceptibility, mineral grains were covered with precipitates and both the surfaces of the minerals and the precipitates were dominated by a Fe-containing phase (Figures 8a–d). In contrast regions of lower magnetic susceptibility had limited precipitation on the surfaces and, although containing a Fe phase, also contained Si, Al, Ca, Na, and Mg (Figures 7a–d). These results are consistent with a previous study at Bemidji by *Baedecker et al*. [1992] who also observed Fe as the main element present on the surface of the mineral grains.

Baedecker et al. [1992] suggested that the magnetite at the Bemidji study site is of authigenic origin. Also, *Tuccillo et al*. [1999] documented that magnetite was abundant in the magnetic fraction of the bulk sediment and represents roughly 0.5% of the bulk sediment, which is consistent with our own results, in addition to siderite and ferroan calcite. Nonetheless, a study by *Zachara et al*. [2004] at the site suggested ferroan calcite precipitation and indicated that they found no evidence of biogenic magnetite formation contradicting the claim made by *Baedecker et al*. [1992] that the magnetite present in the Bemidji aquifer was of biogenic origin. Instead, using the euhedral morphology of magnetite grains, *Zachara et al*. [2004] suggested that the magnetite present in the Bemidji aquifer was detrital magnetite of magmatic or metamorphic origin. Our SEM imaging did not provide conclusive evidence of nano-size magnetite that is typically formed biotically [*Zachara et al*., 2002]. Nonetheless, this could simply be explained by the fact that the SEM imaging was not able to detect the nano-sized particle, if these particles formed as a coating on the surface of the sand particles. In fact, using the Scherrer equation [*Langford and Wilson*, 1978] and the magnetite peak (full width at half maximum) from the XRD spectrum, we calculated crystallite sizes ranging from 30 to 180 nm. We speculate that the sediment was probably coated with magnetite nanoparticles, too small to be seen using the SEM. This could also explain why the EDS analyses from the high magnetic susceptibility zone (Figures 8b and 8c) showed the surface consisting mostly of a Fe phase.

Figures 3 and 4 demonstrate that there is an increase in the magnetic mineral content within the contaminated locations (especially within the free phase plume) and that the magnetic mineral concentration increases toward the top of the water table at the oil/water interface. We also observed a decrease in the magnitude of this response away from the free product zone to the uncontaminated zone (Figures 3 and 4). The coincidence of magnetic susceptibility peaks in zones of hydrocarbon contamination and the spatial variability of the magnitude of the magnetic susceptibility with hydrocarbon distribution points to a possible microbial mediated origin of the magnetic minerals. In this case, the magnetic minerals form abiotically but with the geochemical conditions resulting in the precipitation of theses minerals mediated by microbial iron reduction.

Our findings are consistent with recent results obtained by *Rijal et al*. [2010, 2012] for hydrocarbon-contaminated sites in the Czech Republic. In the *Rijal et al*. [2010] study, the shape and spatial relation between the magnetic anomaly and water table is remarkably similar to the data presented in Figures 3 and 4. *Rijal et al*. [2010] also documented that magnetic concentration parameters increased toward the top of the water table and that the magnetic fractions contained both superparamagnetic and single domain magnetite. Incidentally, *Klueglein et al*. [2013] have recently isolated a new Fe(III)-reducing and magnetite-producing bacterial strain *Geothrix fermentans* HradG1 from the high magnetic and redox-dynamic layer observed in the

Rijal et al. [2010] study. In another study, *Rijal et al*. [2012] documented enhanced magnetite content in hydrocarbon-contaminated samples compared to noncontaminated soils and sediments, suggesting microbial Fe(III) reduction as the possible cause for the enrichment in magnetite within the zone of contamination. At our study site, recent microbial studies have identified the presence of *Albidiferax* (an Fe(III) reducing bacteria), *Geobacter* and *Desulfosporosinus* sp (that is also known to reduce iron) in addition to methanogens and syntrophic bacteria in the zone of enhanced magnetic susceptibility [*Beaver et al*., 2013]. Thus, the microbial results support the idea of a microbial-mediated origin of magnetite across the contaminated plume.

5.2. Fe(II) Concentration Control on MS Variability

Tuccillo et al. [1999] and *Amos et al*. [2012] have documented reduced levels of Fe(III) in the sediments closest to and underneath the oil body (zone 3) whereas Fe(II) values under the oil body (19.2 μmol/g) are as much as 4 times higher than those in the background sediments (4.6 μmol/g) (zone 1). Figure 9 shows that the dissolved Fe(II) concentrations are highest within the free phase oil plume (~ 0.716 mmol/L) within the upper parts of zone 3 and lower parts of zone 8 compared to the dissolved phase plume (less than 0.072 mmol/L; zones 4 and 5). Iron data by *Bekins et al*. [2001] suggests that Fe(II) builds up in excess of Fe(III) near the water table in the oil body (zone 3). Moreover, the reduction in permeability toward the water table can reduce the Fe(II) flow rate, which can increase the chance of Fe(II) complexation by organic matter [*Bekins et al*., 2001]. Incidentally, the peaks in Fe(II) in sediments from *Bekins et al*. [2001] line up with peaks in the magnetic susceptibility profile located at the oil/water interface from borehole G906 (data not shown). Electron mass balance calculations within the Bemidji aquifer by *Amos et al*. [2012] suggest that CH_4 oxidation may be coupled to Fe(III) reduction. In this scenario, CH_4 oxidation linked to Fe(III) reduction within the anaerobic CH_4 plume at the Bemidji site would contribute to the release of Fe(II) and therefore the high concentrations of Fe (II) within the methanogenic zone [*Beal et al*., 2009].

Biomineralization pathways for different iron mineral phases are controlled by many factors including pH, redox potential, carbonate concentration, and mostly, respiration-driven Fe(II) supply rate and magnitude [*Fredrickson et al*., 1998; *Zachara et al*., 2002]. Reaction of Fe(II) with ferrihydrite results in different secondary mineralization pathways including goethite, lepidocrocite, and magnetite. These phases vary in their precipitation extent, rate, and residence time, all of which are primarily a function of Fe(II) concentration and ligand type (Cl, SO_4, CO_3). While lepidocrocite and goethite precipitate over a wide Fe(II) concentration range, magnetite and siderite accumulation is only observed at surface loadings greater than 1.0 mmol Fe(II)/g ferrihydrite (in the absence of bicarbonate). In a laboratory experiment, *Zachara et al*. [2002] investigated the biomineralization of poorly crystalline Fe(III) oxides by dissimilatory metal-reducing bacteria (DMRB). They observed that the supply rate and total concentration of biogenic Fe(II) are the primary determinants of the nature of secondary mineralization products. At lower supply rates, they observed the precipitation of Fe(III) oxides, while at medium and higher rates, magnetite and siderite were dominant precipitates, respectively. *Hansel et al*. [2003] and *Sumoondur et al*. [2008] showed in controlled experiments that, as a function of Fe(II) concentration and ligand type (Cl, SO_4, CO_3), magnetite can be the end-product of a process that may proceed via intermediate phases such as lepidocrocite, goethite, and sulphate green rust. Additionally, *Hansel et al*. [2005] documented the precipitation of magnetite when the Fe(II)/ferrihydrite ratio is greater than 1.0 mmol Fe(II)/g ferrihydrite. *Hansel et al*. [2003] observed the formation of goethite and magnetite by sorption of Fe(II) to ferrihydrite.

To evaluate the role of Fe(II) in the formation of the magnetic mineral phases, we superimposed the magnetic susceptibility profiles on the Fe(II) concentrations measured in the aquifer (Figure 9). We observe that although hydrocarbon contamination exists and iron reduction is taking place over the entire aquifer underneath (i.e., within impacted regions of the aquifer), the enhancement in the MS values occurs only within the zone of highest Fe(II) concentration ($>$0.716 mmol/L) within zone 3, compared to lower magnetic susceptibility values downgradient ($<$0.072 mmol/L). As predicted by *Hansel et al*. [2003, 2005], magnetite accumulation should only be observed at concentrations exceeding 0.3 mmol/L (equivalent to 0.5 mmol Fe (II)/g ferrihydrite), which is consistent with our magnetic susceptibility observations and magnetic mineral quantification. *Hansel et al*. [2003] further report that lower initial Fe(II) concentrations followed by higher concentrations promote goethite accumulation while inhibiting magnetite precipitation even when Fe(II) concentrations increase later on. Thus, the presence of higher concentrations of magnetite in zone 3 suggests

higher initial concentrations and supply rates of Fe (II) within the oil plume and confirms the stable nature of the precipitated magnetite. Therefore the intrusive or nonintrusive measurements of the magnetic susceptibility may provide important insights into the biogeochemical controls and the kinetics and mechanisms of magnetite formation and other magnetic mineral phases.

5.3. Organic Carbon Concentration Control on Magnetic Susceptibility Variability

Figures 3 and 4 show high magnetic susceptibility values within the free phase plume that decrease in magnitude toward the dissolved plume. The high magnetic susceptibility within the free phase plume is only limited to the upper parts of zone 3 and lower parts of zone 8 (Figure 3) where the highest concentrations of hydrocarbons including free phase oil and methane are observed. *Rijal et al*. [2010] made similar observations at another hydrocarbon-contaminated site. The coincidence between the zone of magnetic susceptibility enhancement and the high concentrations of hydrocarbons suggests the coupling of organic carbon oxidation with iron reduction. It also indicates a relationship between the hydrocarbon content and the concentration of Fe(II). *Zachara et al*. [2002] observed in experiments on microbial iron reduction that, when an electron donor (hydrocarbon in our case) was in excess, the ferrihydrite was almost fully transformed to fine-grained magnetite. This process may be similar to the situation near the oil body. Also, *Rijal et al*. [2012] indicated a reasonable relationship between the mass of total nonpolar hydrocarbon (TNPH) and the magnetic susceptibility enhancement in soils.

Organic carbon content may also account for the variability in magnetic susceptibility within the vadose zone across the site. In Figures 3 and 4, the magnetic susceptibility in the vadose zone above the free product plume (geochemical zones 7 and 8 in Figure 2) is enhanced in contrast to that above the dissolved plume (geochemical zone 6 in Figure 2). Figure 9 shows that the magnetic susceptibility enhancement is limited to the zone of the methane plume in the vadose zone. In *Mewafy et al*. [2011], we documented that the enhancement in the magnetic susceptibility values above the free phase plume occurred within a zone where methane depletion was occurring. We further suggested that the formation of magnetic mineral phases provided evidence for the coupling of methane oxidation with iron reduction, which is consistent with recent findings reported for the saturated zone by *Amos et al*. [2012].

5.4. Water Table Fluctuations Control on MS Enhancement

A significant observation in this study is that the enhanced magnetic susceptibility layer occurs entirely within the highest and lowest water mark (Figure 3), suggesting that water table fluctuations have a strong control on biogeochemical processes resulting in magnetic mineral transformation. Similar observations have been made by *Rijal et al*. [2010] during a bioremediation experiment at a hydrocarbon-contaminated site in the Czech Republic. They retrieved core samples from three locations. Two of the cores (S1, S2) were directly affected by groundwater fluctuations during the remediation process, while the third (S3) was less affected. They observed a more than fivefold increase in the magnetic parameters within the zone of WT fluctuation in cores S1 and S2, while this trend was much weaker in S3. They suggested that the zone of water table fluctuation was most biologically active and resulted in a zone of enhanced magnetic susceptibility.

The water table interface can provide large redox gradients between highly reducing conditions below the water table and oxidizing conditions above the water table [e.g., *Revil et al*., 2010]. Fluctuations in the water table may result in large temporal variations in redox conditions [*Vorenhout et al*., 2004]. *Rainwater et al*. [1993] investigated the effect of water table movement on diesel degradation in a soil column versus a static control soil column. They observed that the column subjected to water table movement had 15% less residual diesel than the static control soil column after 9 weeks. A laboratory investigation by *Dobson et al*. [2007] showed that water table fluctuation resulted in the entrapment of light nonaqueous-phase liquid and air below the water table and thus enhanced biodegradation. *Lee et al*. [2001] documented seasonal variations in the concentrations of the contaminant and byproducts in soil gas and groundwater of a shallow contaminated aquifer in Korea. They indicated more active biodegradation in summer than in winter and they related this variation to water table fluctuations.

In a recent study, *Rezanezhad et al*. [2014] investigated the effect of water table fluctuation on soil biogeochemical processes. In one soil column, the water table remained stationary at 20 cm below the soil surface, while in the other, the water table oscillated between the soil surface and the bottom of the column. They observed dramatic changes in the redox potentials for the column with oscillating water table between

~700 mV and −100 mV. Interestingly, they found that water table fluctuation resulted in faster depletion of soil organic carbon within the midsection (transition zone) of the fluctuating water table column. They suggested that transient redox conditions enhanced microbial oxidation of soil organic matter, resulting in the enhanced depletion of available organic matter, hence the limiting respiration rate observed at the end of the experiment. Incidentally, the authors also documented that the potential CO_2 production rates were highest in the zone with ~60% moisture content. They suggested that the periodic variations, together with a water saturation level on the order of 60%, resulted in the enhancement of organic carbon mineralization in the transition zone of the fluctuating column and thus enhanced the soil carbon turnover. However, the dryer and wetter conditions prevailing in the upper and lower sections of the column, respectively, may be limiting CO_2 production. Incidentally, other studies have suggested that soil moisture content profoundly influences composition, motility, survival, and activities of microorganisms responsible for degradation of hydrocarbons with a water content of ~50–80% as optimum for maximum rate of biodegradation of aromatic hydrocarbons [*Yadav and Hassanizadeh*, 2011].

For the Bemidji site, the confinement of the magnetic susceptibility enhancement to the zone of water table fluctuation suggests to us that perhaps this interval may have optimum water saturation conditions necessary for producing maximum rates of biodegradation. In addition we offer an explanation for the peak magnetic susceptibility values occurring at the highest or lowest water mark. Studies from many oil reservoirs have observed degradation-related compositional gradients with the most degraded oil occurring near oil-water contacts, suggesting that the base of the oil column (oil water contact) provides conditions that are most conducive for biodegradation [*Head et al*., 2003; *Bennett et al*., 2013; *Wang et al*., 2013]. The hydrocarbons present in the oil column above the water table provide an abundant supply of electron donors, whereas, the water column below provides the nutrients required for microbial growth, enhancing the activity of the microorganism at the oil-water interface [*Head et al*., 2003]. This process would result in high Fe(II) supply rates and therefore the formation of magnetite as predicted by the *Hansel et al*. [2003, 2005] studies. Thus, the position of the oil-water interface, which fluctuates with the water table position, may explain the peaks in magnetic susceptibility observed at the high and low water table marks and explain why the magnetic susceptibility enrichment is not observed over the entire contaminated aquifer even though the aquifer has high concentrations of organic carbon and Fe(II). In addition, magnetite is a mixed valence mineral containing both Fe(II) and Fe(III). The changing redox conditions imparted by the oscillating water table will favor magnetite formation and therefore the high magnetic susceptibility observed within this zone consistent with our results and those of *Rijal et al*. [2010].

Previous biogeophysical studies at hydrocarbon-contaminated sites have pointed out that the smear zone (within the zone of fluctuating water table) is the most biogeochemically active zone [*Werkema et al*., 2003; *Atekwana et al*., 2004; *Abdel Aal et al*., 2006]. In the above studies a clear enhancement in the bulk electrical and complex conductivity was observed to have occurred within this zone. The conductive signature was purported to result from enhanced mineral weathering from metabolic byproducts such as organic acids [*Atekwana et al*., 2000, 2004; *Sauck*, 2000; *Werkema et al*., 2003], the formation of biofilms, or an increase in surface roughness and surface area [*Abdel Aal et al*., 2006]. In the presence of electron donors and acceptors, this zone may be the source of electrical currents generating electrical field anomalies [*Naudet et al*., 2003, 2004; *Revil et al*., 2010]. In this study, we provide an additive explanation highlighting the role of bio-metallic mineral phases. We suggest that the precipitation of bio-metallic minerals resulting from microbial redox processes can explain the conductive response observed at many hydrocarbon-contaminated sites. In fact, *Mewafy et al*. [2013] documented an enhancement of the complex conductivity response within the magnetite enriched layer and demonstrated through controlled laboratory experiments that the imaginary conductivity component was directly related to the magnetite concentration suggesting that the presence of the magnetite controlled the imaginary conductivity response. Thus, the interpretation of geophysical data at hydrocarbon-contaminated sites must be completed in concert with an understanding of the biogeochemical and terminal electron acceptor processes occurring at the site.

6. Conclusions

We investigated variations in magnetic susceptibility across an oil-contaminated site undergoing active biodegradation with iron reduction and methanogenesis as the dominant biogeochemical processes occurring in

the aquifer. Our results show the following: (1) the presence of an enhanced zone of magnetic susceptibility, which is most likely related to magnetic mineral enrichment, occurring within the zone of water table fluctuation, showing peak values occurring at the top of the water table fluctuating zone and corresponding to the oil-water interface. Such anomalous magnetic susceptibilities are not observed at the background locations; (2) magnetic susceptibility values within the free product plume are generally higher compared to values within the dissolved product plume; (3) magnetic susceptibility values in the vadose zone above the free product plume where methane oxidation is taking place are higher compared to vadose zone samples above the dissolved product plume; (4) high magnetic susceptibility values (90 to 140×10^{-4} SI) coincide with zones of elevated Fe (II) concentrations limited to the upper parts of the water table; and (5) SEM imaging of the surfaces of the mineral grains within the zone of high magnetic susceptibility show coatings of an Fe-containing phase and XRD analyses suggest that magnetite was the dominant magnetic mineral.

We suggest that under high organic carbon loading conditions, a fluctuating water table regime, optimum moisture conditions, and fluctuating redox conditions accelerate microbial activity. Hence, organic carbon degradation results in high rates of Fe(II) production and favors the precipitation of magnetic minerals. The recognition of the zone of enriched bio-metallic magnetic mineral phases within the water table fluctuating zone calls for a reevaluation of biogeophysical signatures observed at organic carbon-rich environments (e.g., hydrocarbon and landfill sites) commonly attributed to an enhancement of pore water conductivity related to the production of metabolic byproducts. We conclude that magnetic susceptibility measurements are: (1) a low-cost, rapid monitoring tool for assessing the extent of hydrocarbon contamination, (2) able to delineate zones where magnetic mineral formation is occurring, and (3) can serve as a proxy for regions where carbon cycling is linked to iron cycling. As a result, biogeophysical studies can play a critical role in delineating zones of enhanced biogeochemical processes so that they can be better studied by microbial and geochemical investigations.

Acknowledgments

This material is partially based on work supported by Enbridge Energy (Ltd.), the Minnesota Pollution Control Agency, and the U.S.G.S. Toxic Waste Substances Program. We thank W. Herkalrath, F. Day-Lewis, J. Lane, M. Erickson, B. Bekins, and J. Trost (U.S.G.S.), J. Heenan and C. Zhang (Rutgers-Newark) for valuable field support and discussions. The U.S. EPA Office of Research and Development funded and collaborated in the research described here under EP-10-D-000488. It has been subjected to Agency review and approved for publication. The authors acknowledge funding from Chevron Energy Technology Company (grant CW852844) and use of Oklahoma State University's XRD Core Facility. Funding for the SEM was provided by NSF grant EAR-0722410. The manuscript benefitted substantially from the constructive comments provided by two anonymous reviewers and the Editors. This is the Boone Pickens School of Geology contribution #2013-8.

References

Abdel Aal, G. Z., L. D. Slater, and E. A. Atekwana (2006), Induced-polarization measurements on unconsolidated sediments from a site of active hydrocarbon biodegradation, *Geophysics*, *71*(2), H13–H24.

Amos, R., B. Bekins, I. Cozzarelli, M. Voytek, J. Kirshtein, E. Jones, and D. Blowes (2012), Evidence for iron-mediated anaerobic methane oxidation in a crude oil-contaminated aquifer, *Geobiology*, *10*, 506–517.

Anderson, R. T., and D. R. Lovley (2000), Anaerobic bioremediation of bBenzene under sulfate-reducing conditions in a petroleum-contaminated aquifer, *Environ. Sci. Technol.*, *34*(11), 2261–2266.

Atekwana, E. A., W. A. Sauck, and D. D. Werkema (2000), Investigations of geoelectrical signatures at a hydrocarbon contaminated site, *J. Appl. Geophys.*, *44*(2–3), 167–180.

Atekwana, E. A., D. D. Werkema, J. W. Duris, S. Rossbach, E. A. Atekwana, W. A. Sauck, D. P. Cassidy, J. Means, and F. D. Legall (2004), In-situ apparent conductivity measurements and microbial population distribution at a hydrocarbon-contaminated site, *Geophysics*, *69*(1), 56–63.

Baedecker, M. J., I. M. Cozzarelli, J. R. Evans, and P. P. Hearn (1992), Authigenic mineral formation in aquifers rich in organic material, in *Proceedings of the 7th International Symposium on Water-Rock Interaction*, edited by Y. K. Kharaka and A. S. Maest, pp. 257–261, A. A. Balkema, Rotterdam.

Baedecker, M. J., I. M. Cozzarelli, R. P. Eganhouse, D. I. Siegel, and P. C. Bennett (1993), Crude-oil in a shallow sand and gravel aquifer: 3. Biogeochemical reactions and mass-balance modeling in anoxic groundwater, *Appl. Geochem.*, *8*(6), 569–586.

Beal, E. J., C. H. House, and V. J. Orphan (2009), Manganese- and iron-dependent marine methane oxidation, *Science*, *325*(5937), 184–187.

Beaver, C., S. Rossbach, E. Atekwana, E. Atekwana, F. Mewafy, G. Abdel Aal, L. Slater, D. Ntarlagiannis, and A. Revil (2013), Microbial communities within zones of elevated magnetic susceptibilities, *Second International Bioremediation and Sustainable Environmental Technologies Symposium*, Jacksonville, FL, 10–13 June.

Bekins, B. A., I. M. Cozzarelli, E. M. Godsy, E. Warren, H. I. Essaid, and M. E. Tuccillo (2001), Progression of natural attenuation processes at a crude oil spill site: II. Controls on spatial distribution of microbial populations, *J. Contam. Hydrol.*, *53*(3–4), 387–406.

Bennett, P. C., D. E. Siegel, M. J. Baedecker, and M. F. Hult (1993), Crude-oil in a shallow sand and gravel aquifer 1. Hydrogeology and inorganic geochemistry, *Appl. Geochem.*, *8*(6), 529–549.

Bennett, B., J. J. Adams, N. D. Gray, A. Sherry, T. B. P. Oldenburg, H. Huang, S. R. Larter, and I. M. Head (2013), The controls on the composition of biodegraded oils in the deep subsurface – Part 3. The impact of microorganism distribution on petroleum geochemical gradients in biodegraded petroleum reservoirs, *Org. Geochem.*, *56*, 94–105.

Cozzarelli, I. M., B. A. Bekins, M. J. Baedecker, G. R. Aiken, R. P. Eganhouse, and M. E. Tuccillo (2001), Progression of natural attenuation processes at a crude-oil spill site: 1. Geochemical evolution of the plume, *J. Contam. Hydrol.*, *53*(3–4), 369–385.

Cozzarelli, I. M., B. A. Bekins, R. P. Eganhouse, E. Warren, and H. I. Essaid (2010), In situ measurements of volatile aromatic hydrocarbon biodegradation rates in groundwater, *J. Contam. Hydrol.*, *111*(1–4), 48–64.

Dearing, J. (1994), *Environmental Magnetic Susceptibility*, *Using the Bartington MS2 System*, Chi Publ., Kenilworth.

Delin, G. N., H. I. Essaid, I. M. Cozzarelli, M. H. Lahvis, and B. A. Bekins (1998), Ground water contamination by crude oil near Bemidji, Minnesota, *U.S. Geological Survey Fact Sheet FS*, 84–98.

Dobson, R., M. H. Schroth, and J. Zeyer (2007), Effect of water-table fluctuation on dissolution and biodegradation of a multi-component, light nonaqueous-phase liquid, *J. Contam. Hydrol.*, *94*(3–4), 235–248.

Dunlop, D. J., and Ö. Özdemir (2001), *Rock Magnetism: Fundamentals and Frontiers*, 573 pp., Cambridge Univ. Press, Cambridge and New York.

Eganhouse, R. P., M. J. Baedecker, I. M. Cozzarelli, G. R. Aiken, K. A. Thorn, and T. F. Dorsey (1993), Crude oil in a shallow sand and gravel aquifer: II, *Org. Geochem., Appl. Geochem.*, *8*, 551–567.

Essaid, H. I., B. A. Bekins, W. N. Herkelrath, and G. N. Delin (2011), Crude oil at the Bemidji site: 25 years of monitoring, modeling, and understanding, *Ground Water*, *49*(5), 706–726.

Fredrickson, J. K., J. M. Zachara, D. W. Kennedy, H. L. Dong, T. C. Onstott, N. W. Hinman, and S. M. Li (1998), Biogenic iron mineralization accompanying the dissimilatory reduction of hydrous ferric oxide by a groundwater bacterium, *Geochim. Cosmochim. Acta*, *62*(19–20), 3239–3257.

Hansel, C. M., S. G. Benner, J. Neiss, A. Dohnalkova, R. K. Kukkadapu, and S. Fendorf (2003), Secondary mineralization pathways induced by dissimilatory iron reduction of ferrihydrite under advective flow, *Geochim. Cosmochim. Acta*, *67*(16), 2977–2992.

Hansel, C. M., S. G. Benner, and S. Fendorf (2005), Competing Fe(II)-induced mineralization pathways of ferrihydrite, *Environ. Sci. Technol.*, *39*(18), 7147–7153.

Head, I. M., D. M. Jones, and S. R. Larter (2003), Biological activity in the deep subsurface and the origin of heavy oil, *Nature*, *426*, 344–352.

Jacobs, I. S. (1963), Metamagnetism of siderite ($FeCO_3$), *J. Appl. Phys.*, *34*(4), 1106–1107.

Klueglein, N., T. Lsekann-Behrens, M. Obst, S. Behrens, E. Appel, and A. Kappler (2013), Magnetite Formation by the Novel Fe(III)-reducing Geothrix fermentans Strain HradG1 Isolated from a hydrocarbon-contaminated sediment with increased magnetic susceptibility, *Geomicrobiol. J.*, *30*(10), 863–873, doi:10.1080/01490451.2013.790922.

Langford, J. I., and A. J. C. Wilson (1978), Scherrer after sixty years: A survey and some new results in the determination of crystallite size, *J. Appl. Crystallogr.*, *11*, 102–113.

Lee, C., J. Lee, J. Cheon, and K. Lee (2001), Attenuation of petroleum hydrocarbons in smear zones: A case study, *J. Environ. Eng.*, *127*(7), 639–647.

Lovley, D. (1990), Magnetite formation during microbial dissimilatory iron reduction, in *Iron Biominerals*, edited by R. B. Frankel and R. P. Blakemore, pp. 151–166, Plenum, New York.

Lovley, D. R. (1993), Dissimilatory metal reduction, *Annu. Rev. Microbiol.*, *47*, 263–290.

Lovley, D. R., J. F. Stolz, G. L. Nord, and E. J. P. Phillips (1987), Anaerobic production of magnetite by a dissimilatory iron-reducing microorganism, *Nature*, *330*(6145), 252–254.

Lovley, D. R., M. J. Baedecker, D. J. Lonergan, I. M. Cozzarelli, E. J. P. Phillips, and D. I. Siegel (1989), Oxidation of aromatic contaminants coupled to microbial iron reduction, *Nature*, *339*(6222), 297–300.

Mewafy, F. M., E. A. Atekwana, D. D. Werkema Jr., L. D. Slater, D. Ntarlagiannis, A. Revil, M. Skold, and G. N. Delin (2011), Magnetic susceptibility as a proxy for investigating microbially mediated iron reduction, *Geophys. Res. Lett.*, *38*, L21402, doi:10.1029/2011GL049271.

Mewafy, F. M., D. D. Werkema, E. A. Atekwana, L. D. Slater, G. Z. Abdel Aal, A. Revil, and D. Ntarlagiannis (2013), Evidence that bio-metallic mineral precipitation enhances the complex conductivity response at a hydrocarbon contaminated site, *J. Appl. Geophys.*, *98*, 113–123.

Mortimer, R. J. G., and M. L. Coleman (1997), Microbial influence on the oxygen isotopic composition of diagenetic siderite, *Geochim. Cosmochim. Acta*, *61*(8), 1705–1711.

Naudet, V., A. Revil, J.-Y. Bottero, and P. Bégassat (2003), Relationship between self-potential (SP) signals and redox conditions in contaminated groundwater, *Geophys. Res. Lett.*, *30*(21), 2091, doi:10.1029/2003GL018096.

Naudet, V., A. Revil, E. Rizzo, J.-Y. Bottero, and P. Bégassat (2004), Groundwater redox conditions and conductivity in a contaminant plume from geoelectrical investigations, *Hydrol. Earth Syst. Sci.*, *8*(1), 8–22.

Nevin, K. P., D. E. Holmes, T. L. Woodard, E. S. Hinlein, D. W. Ostendorf, and D. R. Lovley (2005), Geobacter bemidjiensis sp. nov. and Geobacter psychrophilus sp. nov., two novel Fe(III)-reducing subsurface isolates, *Int. J. Syst. Evol. Microbiol.*, *55*(4), 1667–1674.

Parmar, N., Y. A. Gorby, T. J. Beveridge, and F. G. Ferris (2001), Formation of green rust and immobilization of nickel in response to bacterial reduction of hydrous ferric oxide, *Geomicrobiol. J.*, *18*(4), 375–385.

Porsch, K., U. Dippon, M. L. Rijal, E. Appel, and A. Kappler (2010), In-situ magnetic susceptibility measurements as a tool to follow geomicrobiological transformation of Fe minerals, *Environ. Sci. Technol.*, *44*(10), 3846–3852.

Prommer, H., G. B. Davis, and D. A. Barry (1999), Geochemical changes during biodegradation of petroleum hydrocarbons: Field investigations and biogeochemical modelling, *Org. Geochem.*, *30*(6), 423–435.

Rainwater, K., M. P. Mayfield, C. Heintz, and B. J. Claborn (1993), Enhanced in situ biodegradation of diesel fuel by cyclic vertical water table movement: Preliminary studies, *Water Environ. Res.*, *65*(6), 717–725.

Revil, A., C. A. Mendonça, E. Atekwana, B. Kulessa, S. S. Hubbard, and K. Bolhen (2010), Understanding biogeobatteries: Where geophysics meets microbiology, *J. Geophys. Res.*, *115*, G00G02, doi:10.1029/2009JG001065.

Rezanezhad, F., R.-M. Couture, R. Kovac, D. O'Connell, and P. van Cappellen (2014), Water table fluctuations and soil biogeochemistry: An experimental approach using an automated soil column system, *J. Hydrol.*, *509*, 245–256.

Rijal, M. L., E. Appel, E. Petrovsky, and U. Blaha (2010), Change of magnetic properties due to fluctuations of hydrocarbon contaminated groundwater in unconsolidated sediments, *Environ. Pollut.*, *158*(5), 1756–1762.

Rijal, M., K. Porsch, E. Appel, and A. Kappler (2012), Magnetic signature of hydrocarbon-contaminated soils and sediments at the former oil field Hänigsen, Germany, *Stud. Geophys. Geod.*, *56*(3), 889–908.

Sauck, W. A. (2000), A model for the resistivity structure of LNAPL plumes and their environs in sandy sediments, *J. Appl. Geophys.*, *44*, 151–165.

Schink, B. (2005), Principles of anaerobic degradation of organic compounds, in *Environmental Biotechnology: Concepts and Applications*, edited by H.-J. Jördening and J. Winter, pp. 229–257, Wiley-VCH Verlag GmbH & Co. KGaA, Weinheim, Germany.

Sumoondur, A., S. Shaw, I. Ahmed, and L. G. Benning (2008), Green rust as a precursor for magnetite: An in situ synchrotron based study, *Mineral. Mag.*, *72*(1), 201–204.

Tuccillo, M. E., I. M. Cozzarelli, and J. S. Herman (1999), Iron reduction in the sediments of a hydrocarbon-contaminated aquifer, *Appl. Geochem.*, *14*(5), 655–667.

Vorenhout, M., H. G. van der Geest, D. van Marum, K. Wattel, and H. J. P. Eijsackers (2004), Automated and continuous redox potential measurements in soil, *J. Environ. Qual.*, *33*(4), 1562–1567.

Wang, G., T.-G. Wang, B. R. T. Simoneit, and L. Zhang (2013), Investigation of hydrocarbon biodegradation from a downhole profile in Bohai Bay Basin: Implications for the origin of 25-norhopanes, *Org. Geochem.*, *55*, 72–84.

Werkema, D. D., E. A. Atekwana, A. L. Endres, W. A. Sauck, and D. P. Cassidy (2003), Investigating the geoelectrical response of hydrocarbon contamination undergoing biodegradation, *Geophys. Res. Lett.*, *30*(12), 1647, doi:10.1029/2003GL017346.

Yadav, B. K., and S. M. Hassanizadeh (2011), An overview of biodegradation of LNAPLs in coastal (Semi)-arid environment, *Water Air Soil Pollut.*, *220*, 225–239.

Zachara, J. M., R. K. Kukkadapu, J. K. Fredrickson, Y. A. Gorby, and S. C. Smith (2002), Biomineralization of poorly crystalline Fe(III) oxides by dissimilatory metal reducing bacteria (DMRB), *Geomicrobiol. J.*, *19*(2), 179–207.

Zachara, J. M., R. K. Kukkadapu, P. L. Gassman, A. Dohnalkova, J. K. Fredrickson, and T. Anderson (2004), Biogeochemical transformation of Fe minerals in a petroleum-contaminated aquifer, *Geochim. Cosmochim. Acta*, *68*(8), 1791–1805.